This document is confidential and is proprietary to the American Chemical Society and its authors. Do not copy or disclose without written permission. If you have received this item in error, notify the sender and delete all copies.

Bond Compression upon Chain Extension

Journal:	ACS Macro Letters
Manuscript ID	Draft
Manuscript Type:	Letter
Date Submitted by the Author:	n/a
Complete List of Authors:	Sapir, Liel; Duke University, Mechanical Engineering and Materials Science; Duke University, NSF Center for the Chemistry of Molecularly Optimized Networks Brock, James; The University of North Carolina at Chapel Hill, Department of Chemistry Chen, Danyang; Duke University, Mechanical Engineering and Materials Science; Duke University, NSF Center for the Chemistry of Molecularly Optimized Networks Liao, Qi; Institute of Chemistry Chinese Academy of Sciences, Institute of Chemistry Panyukov, Sergey; P. N. Lebedev Physics Institute, Russian Academy of Sciences; Moscow Institute of Physics and Technology, Department of Theoretical Physics Rubinstein, Michael; Duke University, Thomas Lord Department of Mechanical Engineering and Materials Science; Duke University, Departments of Biomedical Engineering, Chemistry and Physics; Hokkaido University, Institute for Chemical Reaction Design and Discovery (WPI-ICReDD); Duke University, NSF Center for the Chemistry of Molecularly Optimized Networks

SCHOLARONE™ Manuscripts

Bond Compression upon Chain Extension

Liel Sapir^{1,2}, James Brock³, Danyang Chen^{1,2}, Qi Liao⁴, Sergey Panyukov^{5,6}, and Michael Rubinstein^{*,1,2,7,8}

¹Thomas Lord Department of Mechanical Engineering and Materials Science, Duke University, Durham, North Carolina 27708, United States ²NSF Center for the Chemistry of Molecularly Optimized Networks, Duke University, Durham, North Carolina 27708 ³Department of Chemistry, University of North Carolina, Chapel Hill, North Carolina 27599, United States ⁴Institute of Chemistry, Chinese Academy of Sciences, Beijing 100190, China ⁵P. N. Lebedev Physics Institute, Russian Academy of Sciences, Moscow, Russia 117924 ⁶Department of Theoretical Physics, Moscow Institute of Physics and Technology, 141700, Russia ⁷Departments of Chemistry, Biomedical Engineering, and Physics, Duke University, Durham, North Carolina 27708, United States ⁸Institute for Chemical Reaction Design and Discovery (WPI-ICReDD), Hokkaido University, N21W10 Kita-ku, Sapporo 001-0021, Japan

ABSTRACT: Extending polymer chains results in a positive chain tension, f_{ch} , due primarily to conformational restrictions. At the level of individual bonds, however, tension f_b is either negative or positive and depends both on chain tension and bulk pressure. In specific systems, this dependence may not be intuitive, whereby f_{ch} increases while f_b decreases, *i.e.*, the entire chain is extended, while bonds are compressed. Specifically, increasing the grafting density of a polymer brush results in chain extension along the direction perpendicular to the grafting surface, while the underlying bonds are compressed. Similarly, upon compression of polymer networks, the extension of chains oriented in the "free" direction increases, while their bonds are getting more compressed. We demonstrate this phenomenon in molecular dynamics simulations and explain it by the fact that the pressure contribution to f_b is dominant over a wide range of network deformations and brush grafting densities.

The response of polymeric materials to mechanical stimuli is of fundamental importance for elastomers and gels under stress, molecular brushes, and polymers under flow. The macroscopic stress in polymer networks is transduced to tension at the level of single chains, as well as the individual chemical bonds. Both chain and bond tension are of great importance: while chain tension results in the elastic response of the material, bond tension affects a multitude of chemical properties. 1 Chemical reactivity, for example, exponentially depends on the bond tension.²⁻⁴ Therefore, relatively small changes in the bond tension, on the order of several percent, can change bond lifetime by orders of magnitude⁵ and affect the behavior of biological systems. In polymers, the average bond tension depends on both its local environment, i.e. interaction with surrounding molecules, and on the *chain tension* itself. Bond tension in specific sections of molecules is also a control characteristic in the design of singlemolecule sensors, self-healing, or active materials, and determines the overall stability of polymers under externally applied forces. For example, incorporating mechanophores in a polymer allows for tailored activation upon reaching a specific bond tension.^{6,7} Understanding the relationship between bond and chain tensions is thus of fundamental importance.

Differences between Chain and Bond Tension: Chain tension, $\overrightarrow{f_{ch}}$, is defined as the rate of change of the chain free energy F_{ch} with respect to its end-to-end vector \overrightarrow{R}

$$\overrightarrow{f_{ch}} = \partial F_{ch}(\overrightarrow{R})/\partial \overrightarrow{R}. \tag{1}$$

Chain free energy includes both entropic contribution due to variation of polymer conformations and energetic contribution due to the deformation of bonds along the chain. In some cases, chain tension is not uniform but varies along the chain. For example, in polymer brushes, the tension in the grafted chain is ACS Paragon Plus

highest near the grafting point and low near the free end.^{8,9} Another example is a polyelectrolyte chain in dilute solution, with tension induced by intramolecular electrostatic repulsion that is highest in the middle of the chain and lowest near chain ends. 10 Other examples of non-uniform tension are related to friction induced by a polymer moving with respect to surrounding media and include a polymer in elongational flow¹¹ and a polymer pulled through the solution¹². In all these cases of non-uniform tension, the definition in Eq. 1 applies to polymer sections of size R small enough to have an almost constant tension, but larger than the Kuhn segment, so that F_{ch} is still well-defined. Examples of uniform chain tension include polymers stretched by equal and oppositely directed forces applied to their ends, such as unentangled network strands or polymers stretched by optical or magnetic tweezers, see inset in Fig. 1a. In these cases, the average chain tension is equal to the externally applied force with magnitude $f_{ch} = f_{ext}$. Below we will describe the stretching case and will hence use f_{ch} and f_{ext} interchangeably.

The force-extension curve, Fig. 1a, is measured experimentally by the single-molecule force spectroscopy technique. For external forces lower than kT/b, where kT is the thermal energy and b is the Kuhn length, the chain tension arises primarily due to restrictions on polymer conformations and is therefore predominantly entropic. In the θ -solvent or the melt state in this regime $f_{ext} \ll kT/b$, the polymer behaves as a Gaussian chain

$$f_{ch} = \frac{3kT}{Nb^2} \langle R_z \rangle \tag{2}$$

where N is the number of Kuhn segments, and $\langle R_z \rangle$ is the average projection of the chain end-to-end vector onto the direction of the applied force. At tensions higher than $\sim kT/b$, ($\sim 4pN$ for b=1nm) the force-extension dependence becomes strongly non-linear due to the finite extensibility of the chain but is still environment

primarily entropic. At still higher external forces, the enthalpic contributions to the elasticity due to bond deformation become dominant.

Bond tension is fundamentally different from chain tension. For a chemical bond of length l, the instantaneous bond tension is defined as $f_b(l) = \partial U_b(l)/\partial l$, Fig. 1b, where $U_b(l)$ is the bond potential (Fig. 1b, inset). The average bond tension is therefore $\langle f_b \rangle = \langle \frac{\partial U_b}{\partial l} \rangle$ (3)

where the brackets represent the time average with an averaging window larger than the relaxation time of pressure and chain conformations. The deformation characteristics of the bond are determined by its stiffness $\kappa = \partial^2 U_b/\partial l^2$. To compare different bonds, it is useful to introduce the dimensionless stiffness parameter, $S = \kappa \langle l \rangle^2/kT$, where $\langle l \rangle$ is the equilibrium bond length. For example, for a carbon-carbon covalent bond $S \approx 4 \cdot 10^3$, and for a silicon-oxygen bond $S \approx 2 \cdot 10^3$. The value of S determines the relative amplitude of fluctuations of the bond length and instantaneous bond tension. The average bond tension can be roughly estimated by assuming that the cohesive energy associated with molecular attraction in a liquid state exceeds $-\frac{3}{2}kT$, 15 which for a bond of $l \approx 1$ Å suggests $\langle f_b \rangle \approx -60pN$.

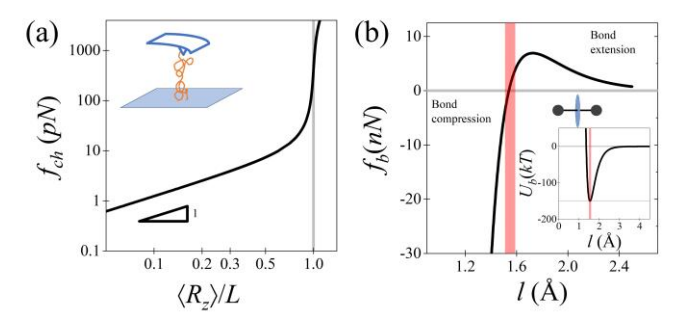


Figure 1. (a) Schematic of a force-extension curve, depicting chain tension, f_{ch} , as a function of the average extension normalized by the undeformed contour length L. The curve corresponds to the freely-jointed chain (FJC) model¹⁶ with Kuhn length b=1nm. The cartoon illustrates the pulling of a tethered polymer chain by AFM. (b) Schematic of bond tension, f_b , and (inset) energy, U_b as functions of bond length l. The curves correspond to a Morse parametrization of a C-C bond^{5,13} at T=298K. Shaded red areas correspond to the range of bond lengths where the potential is up to kT above the minimum. Cartoon depicts a bond (the black line between two black circles) along with its characteristic $area\ per\ bond$, A (blue oval).

The elasticity of polymer networks is determined by the tension in their strands, *i.e.*, chain tension, f_{ch} . Bond tension is qualitatively different from chain tension in that it also depends on *pressure*. It is therefore important to examine the relation between chain and bond tensions.

Below, we present the results of simulations, where we observe a counterintuitive relationship between chain and bond tensions upon increasing grafting density σ_g of the polymer brush, Fig. 2a. Chain tension increases with σ_g as the chains of a denser brush are more elongated. Surprisingly, however, $\langle f_b \rangle$ decreases with increasing σ_g , Fig. 2c.

A similar phenomenon is observed in biaxially compressed elastomers, as shown schematically in Fig. 2b for the network extended along the unconstrained (vertical) direction by a deformation ratio λ_z . As a result, chains oriented along an unconstrained direction are extended with f_{ch} increasing with λ_z , Fig. 2b-c. Naively, one would expect that $\langle f_b \rangle$ in these chains oriented in the "free" z-direction would also increase, but we show herein that $\langle f_b \rangle$ decreases in compressed networks, Fig. 2b-c.

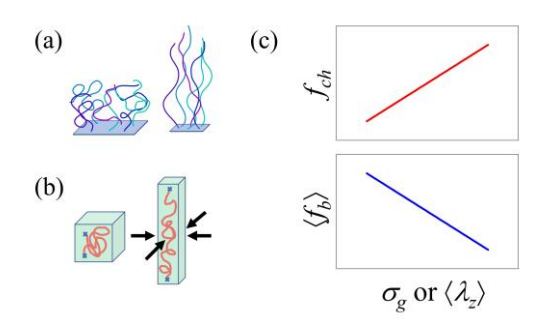


Figure 2. (a) Upon increasing brush grafting density, σ_g , the elongation of chains along the vertical direction increases. (b) The same phenomenon is encountered in the case of the biaxial compression of a polymer network. A strand of a biaxially compressed network oriented in the "free" vertical z-direction is, on average, extended along this direction by the deformation ratio λ_z . (c) The chain tension increases due to chain elongation with increasing σ_g and λ_z for brushes and networks, respectively (top). However, the bond tension decreases, due to increasing pressure (bottom).

We explain this counterintuitive result by accounting for the dependence of the bond tension on both chain tension and pressure, *P*. We discuss this phenomenon for compressed polymer networks as well as with increasing grafting density in polymer brushes. Our theoretical predictions are compared with the results of molecular dynamics simulations of the Kremer-Grest bead-spring model of networks and brushes, ^{19,20} see Section S1 in the Supporting Information (SI) for simulation details.

Contributions to Bond Tension: The average bond tension, $\langle f_b \rangle$, is composed of several contributions, see ref ²¹ and section S2, $\langle f_b \rangle = \langle f_b^{inh} \rangle + \langle f_b^{ch} \rangle + \langle f_b^{int} \rangle$. (4) The $\langle f_b^{inh} \rangle$ term in Eq. 4 is the inherent bond tension that is

The $\langle f_b^{inh} \rangle$ term in Eq. 4 is the inherent bond tension that is due to the orientational/vibrational entropy of the bond and is always positive. This contribution is $\langle f_b^{inh} \rangle = 2kT\langle 1/l \rangle$, where l is the bond length. Note that for stiff bonds with $\kappa \gg kT/\langle l \rangle^2$, $\langle 1/l \rangle \approx 1/\langle l \rangle$. The terms $\langle f_b^{ch} \rangle$ and $\langle f_b^{int} \rangle$, respectively, are due to the bonded and non-bonded interactions of the atoms involved in the bond in question. In the condensed phase, these contributions are negative due to cohesive interactions with neighboring monomers, unless the chain is strongly stretched. The exact differential of $\langle f_b \rangle$ as a function of f_{ch} and pressure can be written as

can be written as
$$d\langle f_b(f_{ch}, P)\rangle = \left(\frac{\partial \langle f_b \rangle}{\partial f_{ch}}\right)_P df_{ch} + \left(\frac{\partial \langle f_b \rangle}{\partial P}\right)_{f_{ch}} dP. \tag{5}$$
We appropriately attack the dependence of band torsion on shain

We separately study the dependence of bond tension on chain tension and on pressure and approximate bond tension by $\langle f_b(f_{ch}, P) \rangle \cong$

$$\langle f_b^0 \rangle + \left[\int_0^{f_{ch}} \frac{\partial \langle f_b \rangle}{\partial f_{ch}} df_{ch} \right]_{P=0} + \left[\int_0^P \frac{\partial \langle f_b \rangle}{\partial P} dP \right]_{f_{ch}=0}, \quad (6)$$

where $\langle f_b^0 \rangle$ is the average bond tension in the unperturbed melt at zero pressure.

Applying an external force to a polymer chain, for example by stretching a tethered chain in solution using an Atomic Force Microscope (Fig. 1a) or by extending a network strand oriented in the "free" direction in an elastomer under compression, increases $\langle f_b \rangle$ in extended chains. This f_{ch} -induced increase in $\langle f_b \rangle$ is equal to the average projection of the external force applied to chain ends onto the direction of the bond and, thus, is proportional to the average cosine of the angle θ between the applied force and the bond vector. This prediction is confirmed by molecular dynamics simulations, in which a single chain in the melt is extended by applying a pair of equal oppositely directed forces f_{ch} to its ends, Fig. 3a. For a freely jointed chain, this increase in bond tension due to the application of chain tension at constant pressure P is proportional to the Langevin function \mathcal{L}^{16}

$$\left[\int_{0}^{f_{ch}} \frac{\partial \langle f_{b} \rangle}{\partial f_{ch}} df_{ch}\right]_{P} = \langle f_{b}(f_{ch}, P) \rangle - \langle f_{b}(0, P) \rangle$$

$$\cong f_{ch} \mathcal{L}(f_{ch}b/kT). \tag{7}$$
This contains in (Fig. 7)

This contribution (Eq. 7) scales quadratically with f_{ch} at low forces, $f_{ch} \ll kT/b$, and linearly with f_{ch} at high forces $f_{ch} \gg kT/b$. The prediction of Eq. 7 with the Kuhn length of the chain, $b = 1.78 \, \sigma$, overestimates the simulation data, while the phenomenological value of $b = 0.7\sigma$ yields good agreement. We explain this difference in Kuhn lengths in Section S3.

The simulation results presented in Fig. 3b confirm the expectation that increasing pressure applied to the polymer melt at constant chain tension compresses the bonds and thereby decreases $\langle f_b \rangle$. This negative contribution to $\langle f_b \rangle$ (the third term in the rhs of Eq. 6) varies almost linearly with applied pressure

$$\left[\int_{0}^{P} \frac{\partial \langle f_{b} \rangle}{\partial P} dP\right]_{f_{ch}} = \langle f_{b}(f_{ch}, P)\rangle - \langle f_{b}(f_{ch}, 0)\rangle$$

$$\cong -P \cdot A \tag{8}$$

where *A* is the average area per bond. We note that *A* does not depend on the bonded potential itself, see Section S4, but rather on the bond length and molecular packing.

This approximation for pressure contribution to $\langle f_b \rangle$ with a constant $A = A_0$ is valid over a wide interval of chain tensions, $f_{ch} \lesssim 10 \, kT/\sigma$ and pressures $P \lesssim 10 \, kT/\sigma^3$, as shown by the black line in Fig.3b. At higher pressures, the melt compressibility becomes important and can be accounted for by including a linear correction $A = A_0(1 - P/P_1)$, see the green line in Fig. 3b and Section S5.

The simulation data justify our approximation for the dependence of bond tension on f_{ch} and pressure, Eq. 6, which can be written explicitly as

$$\langle f_b(f_{ch}, P) \rangle \cong \langle f_b^0 \rangle + f_{ch} \mathcal{L} \left(\frac{f_{ch}b}{kT} \right) - PA.$$
 (9)

Bond and Chain Tensions in Polymer Networks The concurrent effect of pressure and f_{ch} on bond tension is of special importance in deformed polymer networks. We demonstrate this relationship by computer simulations of the uniaxial and biaxial deformation of an end-linked polymer network with an average number $\langle n_x \rangle \approx 35$ of beads per network strand (see Section S1).

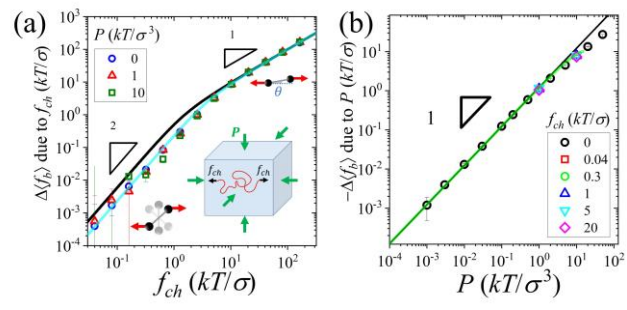


Figure 3. (a) Change in bond tension upon increasing chain tension, f_{ch} , at several constant pressures (P = 0, 1, $10 kT/\sigma^3$, in blue, red, and green, respectively). Top inset: A cartoon depicting a simulation setup where the pressure P on the simulation box is controlled and external pair of forces f_{ext} is applied to the ends of a single chain in the melt, resulting in chain tension $f_{ch} = f_{ext}$. At low chain tension, $f_{ch} < kT/b$, the bonds are weakly oriented and the dependence of $\langle f_b \rangle$ on f_{ch} is quadratic, whereas at high tensions bonds are strongly aligned along the direction of the applied force and the dependence is linear. The black and cyan lines represent fits to the theoretical dependencies in Eq. 7 with $b = 1.78\sigma$ and 0.7σ , respectively (see Section S3 for details). (b) Change in bond tension (with a minus sign) upon increasing pressure, P, at several applied chain tensions. The black line represents the linear prediction of Eq. 8 with constant $A = A_0 = 1.23 \sigma^2$, while the green line corresponds to a pressure-dependent $A = A_0(1 - P/P_1)$ with $P_1 = 34 kT/\sigma^3$ based on isothermal compressibility of the melt (Section S5). Both panels present the results (symbols) obtained from simulations of a polymer melt with chains containing n = 128 beads with full LJ potential (see Section S1).

We compare uniaxial and equi-biaxial network deformations with linear deformation ratios λ_{α} , where $\alpha = x, y, z$. Upon uniaxial deformation along the z direction, $\lambda_z = L_z/L_{z,0}$ is the ratio of the final elastomer length L_z to its initial length $L_{z,0}$, while the other two dimensions, L_x and L_y , are unconstrained under the condition of overall constant pressure P. For equi-biaxial deformation, the deformation ratios $\lambda_x = \lambda_y$ along the x and y directions are controlled, whereby $\langle \lambda_z \rangle$ is the average deformation ratio in the unconstrained z-direction. In our simulations, the ratio of bulk to shear moduli is $\sim 10^3$, implying the Poisson ratio of elastomer is close to $\frac{1}{2}$ and $\lambda_z \cong \lambda_{xy}^{-2}$. We note that for the equi-biaxial deformation, the value of λ_z differed from λ_{xy}^{-2} by less than 1.2% up to $\langle \lambda_z \rangle = 3$. In the following, we compare $\langle f_b \rangle$, the time and ensemble average bond tension over the entire network, and f_{ch} in networks deformed uniaxially and equi-biaxially to a "similar" final shape, i.e., a similar λ_z and thus having similar elastic stress.

The chain tension in each strand of the network is determined from its average end-to-end distance and using the melt fit to the mFJC (Eq. S20) with a tension-dependent Kuhn length (Eq. S21) (see Section S6 for details). As mentioned above, chain tension is independent of pressure (Fig. 3a). Hence, the chain tension f_{ch} averaged over all strands of the network, denoted by \bar{f}_{ch} , does not depend on the specific deformation protocol, as shown in Fig. 4a by comparing identical results of uniaxial and equi-biaxial deformations with the same network shape (same λ_z). The stress-strain curves $\sigma_F(\lambda_z)$ are also identical for such

deformations since the pressure tensor contribution is subtracted from the expression for stress, and hence the stressstrain dependence of the network does not give any indication on the difference in bond tension for different types of deformation (see red and black symbols in Fig. 4a, inset).

In contrast to the identical stress, the pressure inside the elastomer of the same shape under two types of deformations (compression vs stretching at the same λ_z) differs significantly, Fig. 4b. Upon uniaxial extension (black circles for $\lambda_z > 1$) or equibiaxial extension in xy-direction (red triangles for $\lambda_z < 1$), the pressure is negative. In experiments, this negative pressure eventually leads to cavitation and fracture of the material at large deformations.²² In contrast, upon compression, either uniaxial (black circles for $\lambda_z < 1$) or equi-biaxial (red triangles for $\lambda_z > 1$), the pressure is positive, which leads to bond compression. The average chain tension in the unperturbed network, $\bar{f}_{ch,0}$ (at $\lambda_z = 1$) is nonzero due to the stretching of the strands trapped by crosslinks at the preparation conditions. Yet, $\overline{\langle f_b \rangle}$ at $\lambda_z = 1$ and in the unperturbed melt at P = 0 are almost exactly identical (a difference of ~0.1%). See Section S7 for further details.

The positive pressure developed in the network upon compression leads to the decreasing $\overline{\langle f_b \rangle}$ with an increasing λ_z under equi-biaxial compression (red triangles in Fig. 4c) and decreasing $\overline{\langle f_b \rangle}$ upon reducing λ_z for uniaxial compression (black circles in Fig. 4c). These two qualitatively different dependencies $\overline{\langle f_b \rangle}(\lambda_z)$ for uniaxial and equi-biaxial deformations (black and red symbols in Fig. 4c) are in very good agreement with the theoretical prediction (Eq. 9) of the sum of contributions from f_{ch} (Fig. 4a) and P (Fig. 4b) – see red and black solid lines in Figure 4c.

This result reflects the fundamental difference between bond and chain tensions. The chain tension averaged over all strands of the network, \bar{f}_{ch} , increases under network deformation in all cases (the lowest \bar{f}_{ch} is for undeformed networks), but the change in pressure is either positive or negative depending on whether the network is compressed or stretched, respectively. Since bond tension depends strongly on pressure, this results in qualitatively different bond tensions within the networks for compression and stretching protocols, despite the similar network shapes obtained under these deformations.

Since the elastomer shape at a certain λ_z is almost the same for the two deformation protocols, the difference in $\overline{\langle f_b \rangle}$ between them should be dependent only on the pressure difference. Based on Eq. 8, $\overline{\langle f_b \rangle}_{bi} - \overline{\langle f_b \rangle}_{uni} = \Delta P \cdot A$, where we assume a constant A. This prediction (solid line in Fig. 4d) based on the dependence of $\langle f_b \rangle$ on P that we find in the pure melt, Fig. 3b is in excellent agreement with the elastomer simulations, (blue circles in Fig. 4d).

For incompressible affine or phantom networks, the dependence of the tensile stress σ_E on λ_z is predicted to be of neo-Hookean form¹⁶

$$\sigma_E = G(\lambda_z^2 - \lambda_z^{-1}) \tag{10}$$

where G is the shear modulus (black line in Fig. 4a, inset). The corresponding pressure is given by²³

$$P = -\frac{\alpha}{3}\sigma_E = -\frac{\alpha G}{3} \frac{(\lambda_Z^2 + \lambda_Z + 1)}{\lambda_Z} (\lambda_Z - 1)$$
 (11)

where in the last expression we used the stress σ_E given by Eq. 10, and α is a constant equal to 1 and -2 for uniaxial and equibiaxial deformation, respectively. From Fig. 3b we observed

that the pressure contribution to the bond tension varies linearly with pressure (Eq. 8),

$$\left[\int_{0}^{P} \frac{\partial \langle f_{b} \rangle}{\partial P} dP\right]_{f_{ch}} \cong -PA \cong \alpha GA \left[\frac{(\lambda_{z}^{2} + \lambda_{z} + 1)}{3\lambda_{z}}\right] (\lambda_{z} - 1), \quad (12)$$

where the term in the square brackets in the last expression is ~ 1 for small λ_z . Hence, for small deformations the pressure contribution to $\langle f_b \rangle$ depends linearly on the strain, $\lambda_z - 1$. For an affine network of Gaussian chains, the chain tension averaged over all network strands follows

$$\frac{\bar{f}_{ch}}{\bar{f}_{ch,0}} = \sqrt{\frac{1}{3} \left(\frac{2}{\lambda_z} + \lambda_z^2\right)} \approx 1 + \frac{1}{2} (\lambda_z - 1)^2. \tag{13}$$

Therefore, chain tension varies quadratically with strain $\bar{f}_{ch} \sim (\lambda_z - 1)^2$ for small deformations. For small strains, the increase in bond tension $\langle f_b \rangle$ due to increase in chain tension is $\left[\int_0^{f_{ch}} \frac{\partial \langle f_b \rangle}{\partial f_{ch}} df_{ch} \right]_p - \frac{b}{3kT} \bar{f}_{ch,0}^2 \cong \frac{b}{3kT} \bar{f}_{ch,0}^2 (\lambda_z - 1)^2.$ (14)

It follows that at small strain $\lambda_z - 1$, the pressure contribution to the bond tension (varying linearly with strain, Eq. 12) is much larger than the chain tension contribution (varying quadratically with strain, Eq. 14), and is therefore dominant. See Section S7 and Fig. S11 for a comparison of these relative contributions.

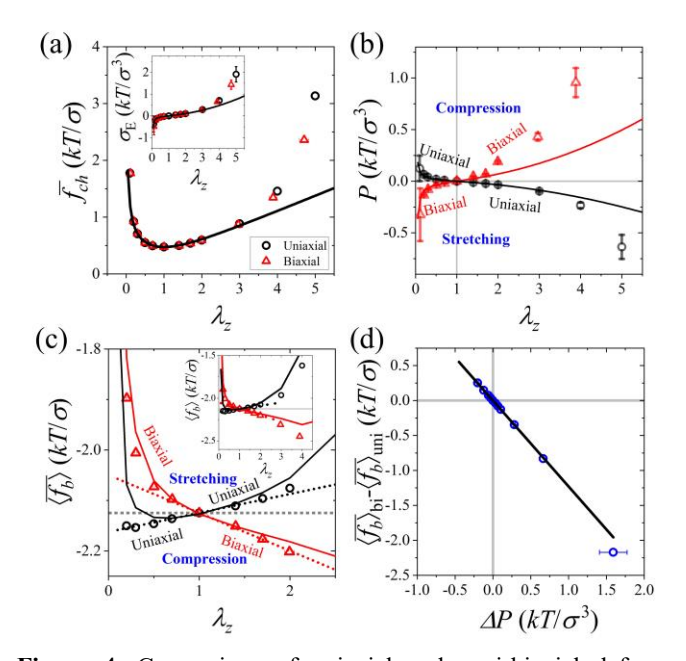


Figure 4. Comparison of uniaxial and equi-biaxial deformations of end-linked elastomer with $\langle n_x \rangle \approx 35$ beads per network strand. (a) Chain tension \bar{f}_{ch} averaged over all network strands as a function of λ_z . The black line is a fit to Eq. 13. Inset: Stress-elongation dependencies. The black line is a fit to the affine prediction, Eq. 10. (b) Pressure as a function of λ_z . Lines correspond to Eq. 11 with shear modulus G =0.03 kT σ^{-3} . (c) Bond tension $\langle f_b \rangle$ averaged over all network strands as a function of λ_z . The solid lines are obtained from Eq. 9 using the measured average chain tension, \bar{f}_{ch} , and the pressure P calculated in the simulations. The dotted lines are predictions of Eq. 12 accounting only for the pressure contribution, with $A = 1.23 \sigma^2$ and $G = 0.03 kT \sigma^{-3}$. Inset: The same data over a broader range of λ_z . (d) The difference between average bond tension $\overline{\langle f_h \rangle}$ for equi-biaxial and uniaxial deformations at the same deformation ratio, as a function of the

pressure difference. The solid line is the prediction based on the linear approximation Eq. 8.

Using the cross-sectional area per bond, $A=1.23~\sigma^2$, determined from a linear fit to Fig. 3b and using the shear modulus $G=0.03~kT~\sigma^{-3}$, determined from Mooney-Rivlin analysis of Fig. 4a, inset, we can successfully predict average bond tension $\overline{\langle f_b \rangle}$ as a function of λ_z for small strains $|\lambda_z - 1| \ll 1$, Fig 4c, dotted lines.

The elongation of strands in a network is inherently heterogeneous. While the pressure is uniform over the whole network, the chain tension depends on the relative extension $\langle R \rangle / L$ of the network strand, where L is the contour length. Hence the bond tension will be different in different network strands, $\langle f_b(\langle R \rangle / L) \rangle$. The distribution of chain tensions will determine the distribution of bond tension across the network. The function $\langle f_b(\langle R \rangle / L) \rangle$ is controlled by the deformation-dependent pressure. We discuss this heterogeneity in Section S7 (Fig. S13).

Summary: Our analyses establish a link between two distinct physical tensions: the chain tension, f_{ch} , which is always positive, and the average bond tension in the polymer chain, $\langle f_b \rangle$, which can be positive or negative. The average bond tension is a function of both chain tension f_{ch} and pressure P. In polymer networks, pressure P makes the dominant contribution to $\langle f_b \rangle$ averaged over all network strands. This results in bonds being on average compressed while chains are extended. However, while pressure is a global thermodynamic variable affecting all bonds similarly, the chain tension is inherently local and depends on the specific network strands involved and their connectivity. For some highly stretched strands, the average bond tension far exceeds its network average.

The same phenomenon is also demonstrated in polymer brushes. With increasing grafting density, σ_g , each chain is extended in the direction normal to the grafting surface. Increasing σ_g induces additional tension in chains. This effect is analogous to the deformations of mesophases of block copolymers upon increasing repulsion between the two blocks. Unlike networks, all chains are on average subjected to the same elongation ratio (their time average of R_z is the same). The increased stress is balanced by increased pressure, which leads to an overall bond compression in a wide range of σ_g (Fig. 2a,c). This observation persists even for swollen brushes and when restricted bond angles are introduced between chain segments. We discuss this in more detail in Section S8.

The average bond tension in the network as a function of chain elongation ratio, $\langle f_b(\langle R \rangle/L) \rangle$, and specifically, the tail of the highly stretched strands (Section S7), has major implications for the reactivity of the system, for example for fracture, ²⁴ and mechanophore activation. Changes in pressure imposed either indirectly by a tensile deformation or by increased hydrostatic pressure can significantly affect bond scission conditions. For example, assuming Arrhenius kinetics, the standard force-dependence of the rate constant ^{1,25} changes by the factor $\exp(-f_b l_a/kT)$, where l_a is the activation length. For a typical bond of $l_a \approx 0.4$ Å at temperature T = 300K, a change of bond tension by 0.1nN, for example by stretching a chain, will modify the rate constant by a factor $\sim e$. Through Eq. 8 we can predict that this change can be counteracted by applying

hydrostatic pressure of $\sim 10^5$ atm, which is attainable in an experimental setup, for example by diamond anvil cells.²⁶

The observed compression of bonds (more negative $\langle f_b(\langle R \rangle / L) \rangle$) upon network compression (either uniaxial or equi-biaxial) reduces the fraction of highly stretched bonds (Fig. S13 and Section S7). This suggests that bond scission is suppressed to higher elongation ratios $\langle R \rangle / L$ than those expected solely from the contribution of chain extension.

Our results also imply that knowledge of the exact dependence of $\langle f_b \rangle$ on both f_{ch} and pressure P allows the determination of chain tension by measuring the bond tension and pressure. This may allow the use of covalent bonds as a molecular gauge for the tension of the entire chain, which will be helpful in the analysis of molecular networks and other polymer architectures.

ASSOCIATED CONTENT

Supporting Information. Details of molecular dynamics simulations, bond tension components, the effect of interactions, bond tension dependence on boding potential, area per bond calculation, the force-extension curve in the melt state, bond tension in elastomers, and detailed brush simulation results. This material is available free of charge via the Internet at http://pubs.acs.org.

AUTHOR INFORMATION

Corresponding Author

* Email: michael.rubinstein@duke.edu

Notes

The authors declare no competing financial interest.

ACKNOWLEDGMENT

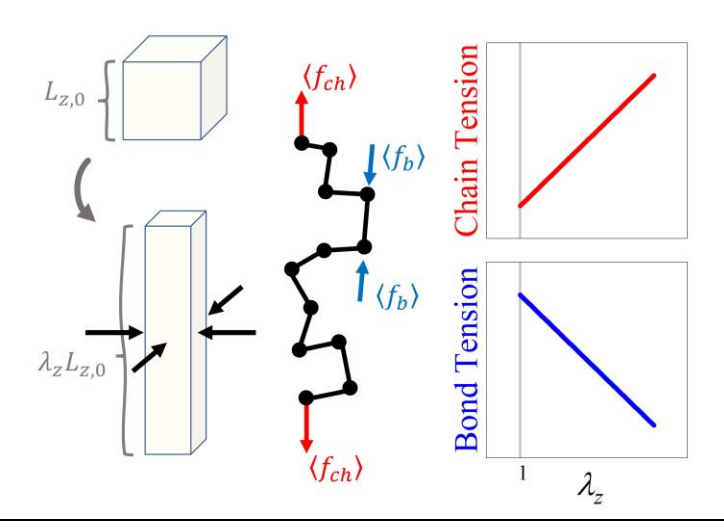
The authors thank Sergei Sheiko for helpful discussions. This work was funded by Duke University, the NSF Center for the Chemistry of Molecularly Optimized Networks (MONET), CHE-2116298, and the Institute for Chemical Reaction Design and Discovery (WPI-ICReDD) at Hokkaido University. Q.L. has received the financial support for this work from the National Natural Science Foundation of China under Grant 21973103.

REFERENCES

- Sheiko, S. S.; Panyukov, S.; Rubinstein, M. Bond Tension in Tethered Macromolecules. Macromolecules 2011, 44 (11), 4520–4529. https://doi.org/10.1021/MA200328H/ASSET/IMA GES/MA-2011-00328H M017.GIF.
- (2) Kauzman, W.; Eyring, H. The Viscous Flow of Large Molecules. J Am Chem Soc 1940, 62 (11), 3113–3125. https://doi.org/10.1021/ja01868a059.
- (3) Bell, G. I. Models for the Specific Adhesion of Cells to Cells. Science (1979) 1978, 200 (4342), 618–627. https://doi.org/10.1126/SCIENCE.347575.
- (4) Zhurkov':'~', S. N. Kinetic Concept of the Strength of Solids. International journal of fracture mechanics 1965 1:4 1965, 1 (4), 311–323. https://doi.org/10.1007/BF03545562.
- (5) Beyer, M. K. The Mechanical Strength of a Covalent Bond Calculated by Density Functional Theory. Journal of Chemical Physics 2000, 112 (17), 7307–7312. https://doi.org/10.1063/1.481330.

- (6) Wang, Z.; Zheng, X.; Ouchi, T.; Kouznetsova, T. B.; Beech, H. K.; Av-Ron, S.; Matsuda, T.; Bowser, B. H.; Wang, S.; Johnson, J. A.; Kalow, J. A.; Olsen, B. D.; Gong, J. P.; Rubinstein, M.; Craig, S. L. Toughening Hydrogels through Force-Triggered Chemical Reactions That Lengthen Polymer Strands. Science (1979) 2021, 374 (6564), 193. https://doi.org/10.1126/SCIENCE.ABG2689/SUPP L_FILE/SCIENCE.ABG2689_MOVIES_S1_AND S2.ZIP.
- (7) Ghanem, M. A.; Basu, A.; Behrou, R.; Boechler, N.; Boydston, A. J.; Craig, S. L.; Lin, Y.; Lynde, B. E.; Nelson, A.; Shen, H.; Storti, D. W. The Role of Polymer Mechanochemistry in Responsive Materials and Additive Manufacturing. Nature Reviews Materials 2020 6:1 2020, 6 (1), 84–98. https://doi.org/10.1038/s41578-020-00249-w.
- (8) Semenov, A. N. Contribution to the Theory of Microphase Layering in Block-Copolymer Melts. Zh. Eksp. Teor. Fiz 1985, 88, 1242–1256.
- (9) Milner, S. T.; Witten, T. A.; Cates, M. E. A Parabolic Density Profile for Grafted Polymers. EPL 1988, 5 (5), 413–418. https://doi.org/10.1209/0295-5075/5/5/006.
- (10) Liao, Q.; Dobrynin, A. v.; Rubinstein, M. Molecular Dynamics Simulations of Polyelectrolyte Solutions: Nonuniform Stretching of Chains and Scaling Behavior. Macromolecules 2003, 36 (9), 3386–3398. https://doi.org/10.1021/ma025995f.
- (11) Rabin, Y. Polymer Fracture in Steady and Transient Elongational Flows. J Chem Phys 1987, 86 (9), 5215–5216. https://doi.org/10.1063/1.452645.
- (12) Ajdari, A.; Brochard-Wyart, F.; Gay, C.; de Gennes, P. G.; Viovy, J. L. Drag on a Tethered Chain Moving in a Polymer Melt. Journal de Physique II 1995, 5 (4), 491–495. https://doi.org/10.1051/jp2:1995145.
- (13) Silberberg, M.; Amateis, P. Chemistry: The Molecular Nature of Matter and Change, 7th ed.; McGraw Hill Education, 2016.
- (14) Oesterhelt, F.; Rief, M.; Gaub, H. E. Single Molecule Force Spectroscopy by AFM Indicates Helical Structure of Poly(Ethylene-Glycol) in Water. New J Phys 1999, 1, 6–6. https://doi.org/10.1088/1367-2630/1/1/006.
- (15) Israelachvili, J. N. Intermolecular and Surface Forces, 3rd ed.; Elsevier: Burlington, MA, 2011.

- https://doi.org/10.1016/B978-0-12-375182-9.10025-9.
- (16) Rubinstein, M.; Colby, R. H. Polymer Physics; Oxford University Press: New York, 2003.
- (17) Doi, M.; Edwards, S. F. The Theory of Polymer Dynamics; Clarendon Press, 1988.
- (18) Gao, J.; Weiner, J. H. Chain Force Concept in Systems of Interacting Chains. Macromolecules 1991, 24 (18), 5179–5191. https://doi.org/10.1021/MA00018A024/ASSET/M A00018A024.FP.PNG V03.
- (19) Grest, G. S.; Kremer, K. Molecular Dynamics Simulation for Polymers in the Presence of a Heat Bath. Phys Rev A (Coll Park) 1986, 33 (5), 3628– 3631. https://doi.org/10.1103/PhysRevA.33.3628.
- (20) Kremer, K.; Grest, G. S. Dynamics of Entangled Linear Polymer Melts: A Molecular-Dynamics Simulation. J Chem Phys 1990, 92 (8), 5057–5086. https://doi.org/10.1063/1.458541.
- (21) Gao, J.; Weiner, J. H. Bond Forces and Pressure in Diatomic Liquids. Mol Phys 1990, 70 (2), 299– 318. https://doi.org/10.1080/00268979000101011.
- (22) Gent, A. N.; Wang, C. Fracture Mechanics and Cavitation in Rubber-like Solids. Journal of Materials Science 1991 26:12 2013, 26 (12), 3392–3395. https://doi.org/10.1007/BF01124691.
- (23) Landau, L. D.; Lifshits, E. M. Theory of Elasticity, 3rd ed.; Pergamon: Oxford, England, 1986.
- (24) Wang, S.; Panyukov, S.; Rubinstein, M.; Craig, S. L. Quantitative Adjustment to the Molecular Energy Parameter in the Lake-Thomas Theory of Polymer Fracture Energy. Macromolecules 2019, 52 (7), 2772–2777. https://doi.org/10.1021/acs.macromol.8b02341.
- (25) Park, I.; Shirvanyants, D.; Nese, A.; Matyjaszewski, K.; Rubinstein, M.; Sheiko, S. S. Spontaneous and Specific Activation of Chemical Bonds in Macromolecular Fluids. J Am Chem Soc 2010, 132 (35), 12487–12491. https://doi.org/10.1021/JA105897B/SUPPL_FILE/ JA105897B SI 001.PDF.
- (26) Meersman, F.; Mc Millan, P. F. High Hydrostatic Pressure: A Probing Tool and a Necessary Parameter in Biophysical Chemistry. Chemical Communications 2013, 50 (7), 766–775. https://doi.org/10.1039/C3CC45844J.



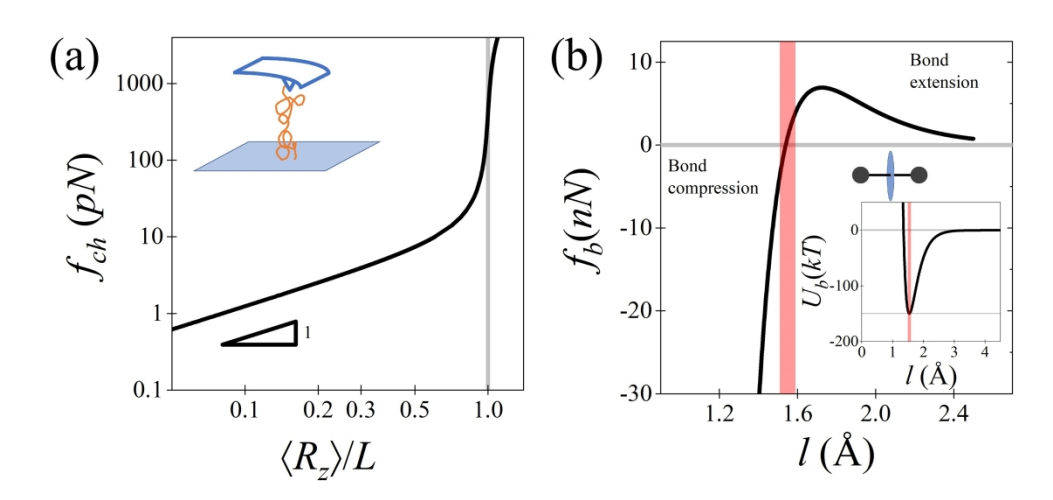


Figure 1
334x161mm (300 x 300 DPI)

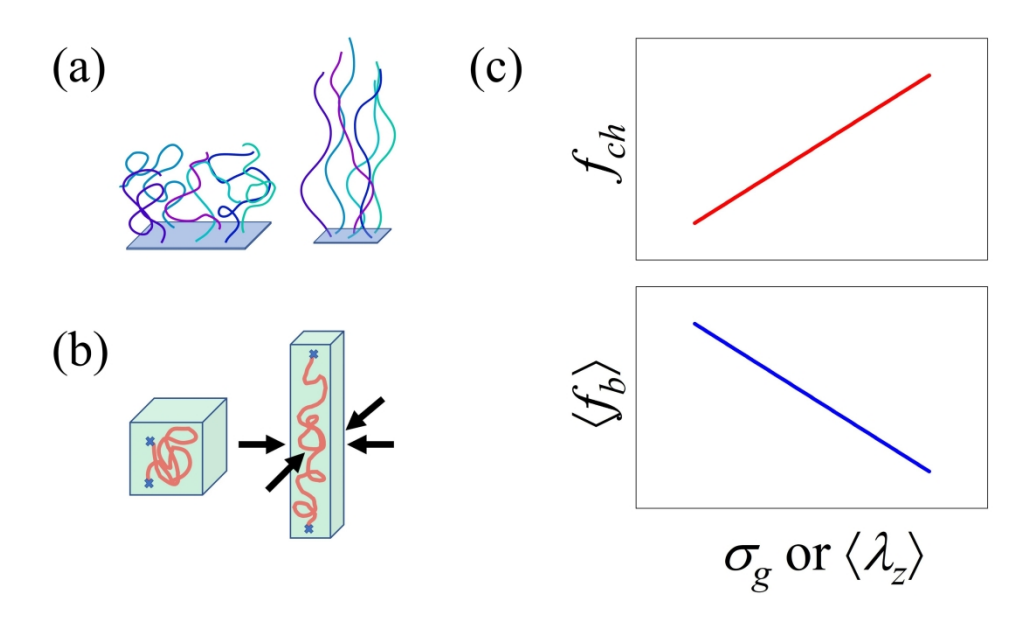


Figure 2 314x190mm (300 x 300 DPI)

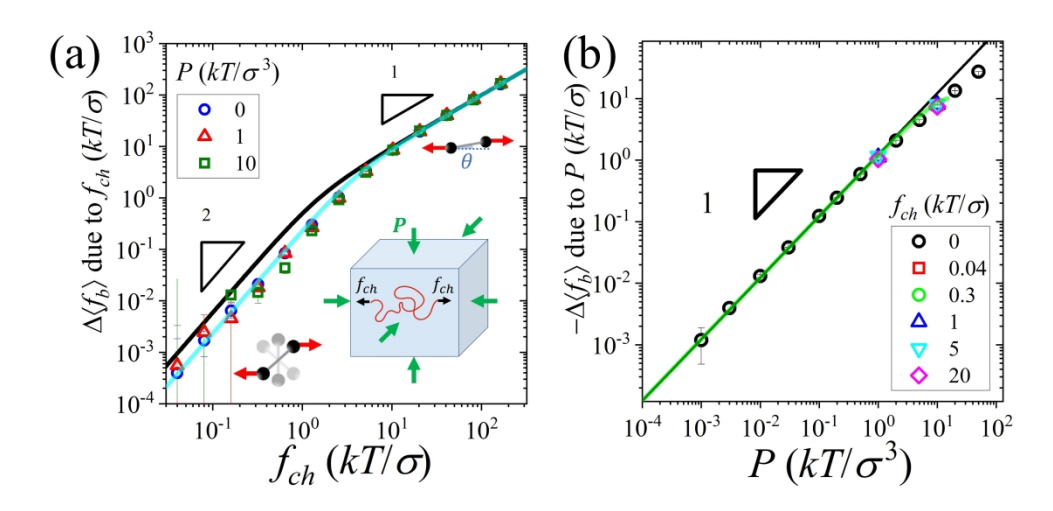


Figure 3 327x162mm (300 x 300 DPI)

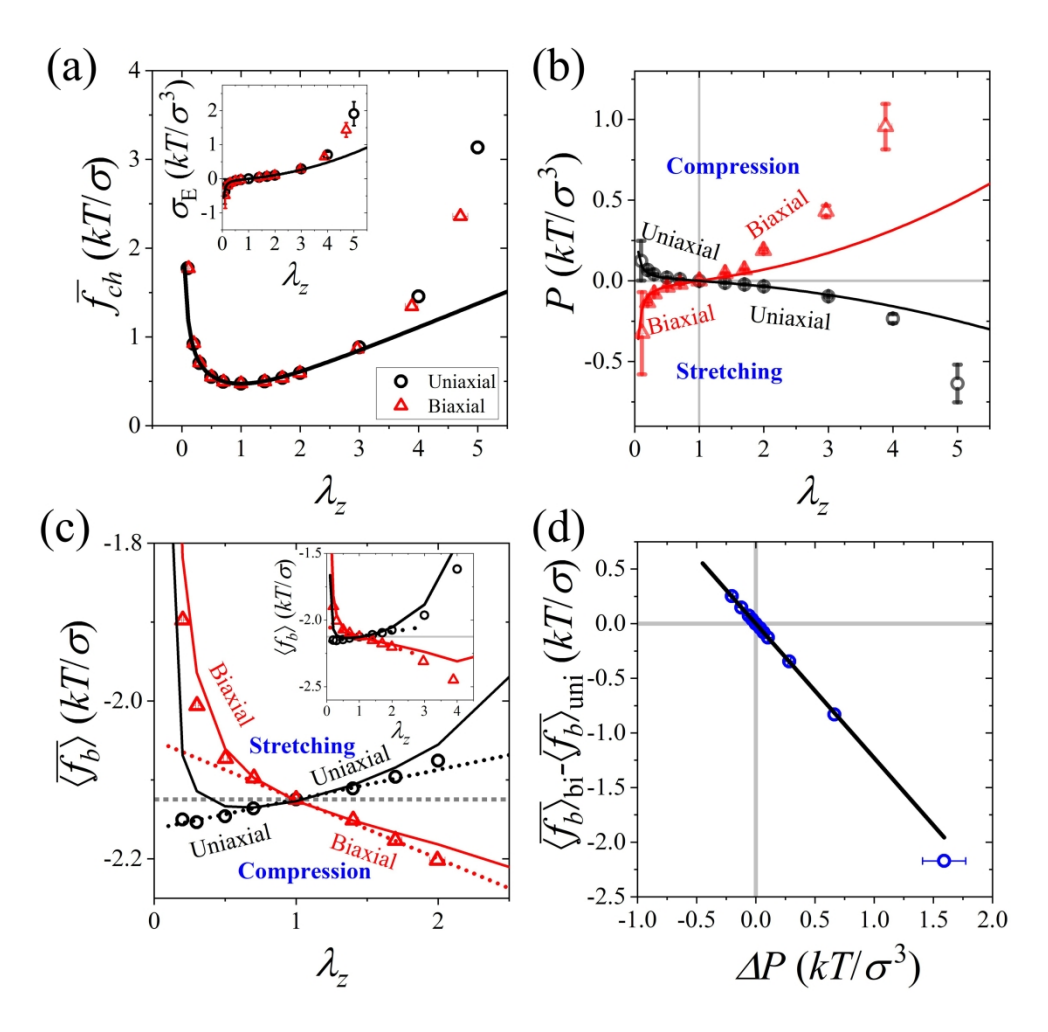
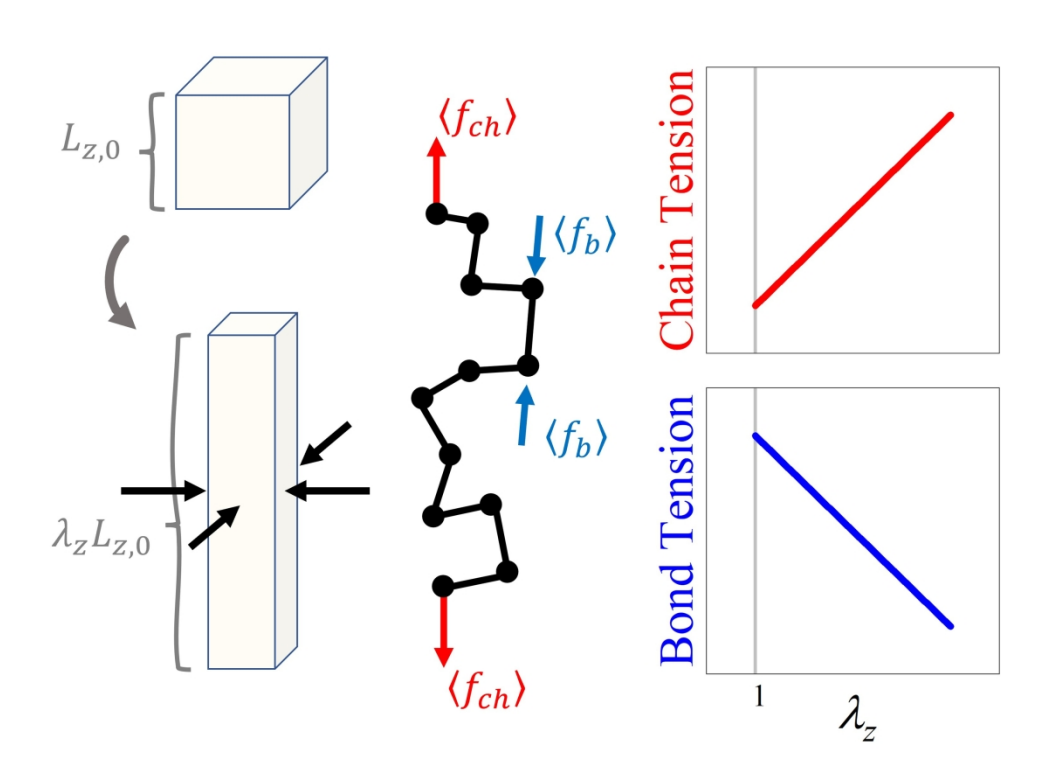


Figure 4
332x324mm (300 x 300 DPI)



TOC Graphic 243x177mm (300 x 300 DPI)